Adaptive and Energy Efficient Walking in a Hexapod Robot under Neuromechanical Control and Sensorimotor Learning

Xiaofeng Xiong, Florentin Wörgötter, and Poramate Manoonpong

***Abstract*—The control of multi-legged animal walking is a neuromechanical process, and to achieve this in an adaptive and energy efficient way is a difficult and challenging problem. This is due to the fact that this process needs in real time 1) to coordinate very many degrees of freedom of jointed legs, 2) to generate the proper leg stiffness (i.e., compliance), and 3) to determine joint angles that give rise to particular positions at the endpoints of the legs. To tackle this problem for a robotic application, here we present a neuromechanical controller coupled with sensorimotor learning. The controller consists of a modular neural network (MNN) for coordinating 18 joints and several virtual agonist-antagonist muscle mechanisms (VAAMs) for variable compliant joint motions. In addition, sensorimotor learning, including forward models and dual-rate learning processes, is introduced for predicting foot force feedback and for online tuning the VAAMs' stiffness parameters. The control and learning mechanisms enable the hexapod robot AMOS to achieve variable compliant walking that accommodates different gaits and surfaces. As a consequence, AMOS can perform more energy efficient walking, compared to other small legged robots. In addition, this study also shows that the tight combination of neural control with tunable muscle-like functions, guided by sensory feedback and coupled with sensorimotor learning, is a way forward to better understand and solve adaptive coordination problems in multi-legged locomotion.**

***Index Terms*—Legged locomotion, bio-inspired robot control, muscle model, variable impedance control.**

I. Introduction

LEGGED animals are capable of adjusting their leg stiffness to accommodate surfaces of variable structural properties [1], [2], thereby leading to adaptive and energy efficient locomotion [3], [4]. They also tune their leg stiffness to accommodate different gaits based on energetic cost [5], [6], [7], [8]. Neurophysiological studies have revealed that these behaviors arise from the interplays between the nervous systems and the musculoskeletal structures (i.e., muscles and body) of legged animals [9], [10], [11]. These neuromechanical interactions [12], [13] govern how legged animals achieve adaptive locomotion on different surfaces. For example, cockroaches rely more on their musculoskeletal structures to move over a regular surface. But moving over a more difficult one, they need to resort to the integrations of their nervous systems and musculoskeletal structures [14].

As Bernstein pointed out, the need to control many degrees of freedom (DOFs) is a characteristics of neuromechanical systems [15], [10]. In a cockroach (e.g., Blaberus discoidalis), for instance, there are 220 muscles controlling legs with at least 19 DOFs that contribute to its locomotion [16]. Owing to this, modeling the cooperations within and between different functional components of neuromechanical systems in legged locomotion is a very challenging task (Bernstein's famous 'degrees of freedom' problem [15], [10]). Along this paradigm, Full and Koditschek proposed a specific solution where two types of dynamic models (i.e., *template* and *anchor*) are used to model legged locomotion with many DOFs [17]. An *anchor* is a representative model with detailed descriptions of neural circuits, muscles, and joints. Whereas, a *template* represents the simplest model of locomotion by trimming away the detailed descriptions (e.g., muscles and joints) of the degrees of freedom. Referring to the *template*, hexapod robots (i.e., RHex robots) were designed by Koditschek and his colleagues [18]. Each RHex robot having only six DOFs showed unprecedented mobility over different surfaces. Besides, they can also achieve energy efficient locomotion by exploiting passive variable compliant legs. For example, leg compliance of a RHex robot was manually tuned to accommodate its running speeds based on energetic cost [19]. The RHex robot is the best example for a coordination architecture controlling faster movement (e.g., running) where mechanical properties (e.g., leg compliance) must be increasingly well tuned to adapt to different environments [20], [10]. In such a case, more feed-forward and decentralized control can suffice, since feedback control may not be effective due to noisy sensing. By contrast, slower movement (e.g., walking) can heavily count on sensing which allows for more adaptive movement [21], [22]. Similarly, here more feedback and a centralized coordination architecture will be utilized to control our hexapod robot AMOS in a neuromechanical manner. Moreover, the modeling of RHex robots is no more than a *template*, since this *template* behavior was not embedded within a very detailed model (i.e., *anchor*). The *anchor* model is a representative model describing a nervous system, muscles, joints, and legs with many DOFs like in insects [20]. *Templates* and *anchors* are more than 'simple models' and 'complex models'. Therefore, there should be a natural embedding of the *template* behavior within the *anchor* [17], [23]. Attempting to embed the *template* within an *anchor*, Holmes *et. al.* [24] presented the com-

X. Xiong, F. Wörgötter, and P. Manoonpong are with Bernstein Center for Computational Neuroscience (BCCN), The Third Institute of Physics, Georg-August-Universität Göttingen, D-37077 Göttingen, Germany. e-mail: xiaofeng.xiong@phys.uni-goettingen.de, worgott@gwdg.de.

P. Manoonpong is also with Center for Biorobotics, Mærsk Mc-Kinney Møller Institute, University of Southern Denmark, 5230 Odense M, Denmark. e-mail: poma@mmmi.sdu.dk.

prehensive models of legged locomotion which integrates a nervous system, central pattern generators (CPGs) [25], muscle dynamics, and body mechanics. Thereinto, a Hill muscle model [26], [27] was adopted to express the force generated by agonist and antagonist muscles where there are up to 26 parameters to be tuned. Thus, such detailed neuromechanical models (i.e., *anchors*) are computationally expensive and not practical for being implemented on physical legged robots. Therefore, a computational model for adaptive and energy efficient physical robot locomotion that accommodates different gaits and surfaces remains an important and unresolved problem in a neuromechanical context [15], [10].

To solve this problem, we propose a neuromechanical controller [21] coupled with sensorimotor learning [28], [29] for active tuning [11] of passive properties (e.g., stiffness parameters) of the muscle-like components driving the joints during locomotion. Specifically, here the multi-legged robot can online adjust the stiffness parameters to produce variable compliant joint motions, thereby accommodating its walking to different gaits and surfaces. Thus, one of the main objectives of this paper is to show that neuromechanical control coupled with sensorimotor learning can generate variable compliant joint motions of a hexapod robot with 19 DOFs, like AMOS. The control and learning mechanisms adopted here enable AMOS to achieve adaptive and energy efficient walking over different surfaces with the appropriate gaits. Generally, energy efficiency is measured by cost of transport[1] COT (i.e., specific resistance [30], [18]). Lower COT corresponds to more energy efficient locomotion. We show that our hexapod robot AMOS can achieve lower COTs (see Table I and Figs.7 in supplementary information) than other small legged robots (less than 8 kg [31]), when proper gaits are chosen for walking over different surfaces. These surfaces include loose surfaces (e.g., fine gravel and coarse gravel), an elastic surface (e.g., sponge), and a muddy surface (e.g., grassland).

Classical neural control [32] and variable compliance control [33] are generalized and integrated into our neuromechanical controller consisting the modular neural network (MNN) and several virtual agonist-antagonist mechanisms (VAAMs). Such an integration facilitates more adaptive and energy-efficient walking on challenging surfaces. For instance, the neuromechanical controller enables AMOS to achieve more energy-efficient waking on the challenging surfaces [21], compared to the adaptive neural controller [22], [58]. This is because the adaptive neural controller consists only of the MMN and adaptive forward models without the muscle-like mechanisms (e.g., VAAMs), which allow for variable compliant joint motions for more energy-efficient walking on the surfaces. Generally, variable compliant joint motions can be achieved by passive or active compliance control. Passive compliance control is typically regarded as the integration of actuators and viscoelastic mechanics [34]. Such control, however, leads to structural and sensory complexities that cause bulkier and energy-inefficient legged robots with many DOFs [35]. Whereas our neuromechanical controller solves these problems virtualizing the muscle-like mechanisms (i.e., VAAMs), which can be applied to variable compliance control of lightweight legged robots with many DOFs. Regardless of additional passive components, the VAAMs or active compliance control is characterized by software control of joint positions or torques [21], [33]. The implementation of active compliance control typically requires force/torque sensing at each joint of legged robots. Whereas the VAAMs make AMOS achieve variable compliant joint motions relying only force sensing at the end effector of its leg. Moreover, the integration of the VAAMs and a proximo-distal gradient enhances stabilities of variable compliant locomotion. Whereas active compliance control intrinsically results in instability of variable compliant locomotion [36], [37]. Furthermore, adaptive compliance control on a physical legged robot with many DOFs remains an important and unsolved problem in a context of energy-efficient walking on different surfaces. Here we develop sensorimotor learning to self-adjust the stiffness parameters of the VAAMs, which adapts AMOS's walking to different gaits and surfaces.

The work presented in this paper is built on the neuromechanical controller where the stiffness parameters of the muscle-like mechanisms (i.e., VAAMs) were manually adjusted with only one gait [21]. Whereas now sensorimotor learning is developed and integrated to self-adjust the stiffness parameters of the VAAMs of the neuromechanical controller, which adapts AMOS's walking to nine gaits and four surfaces. As a result, the neuromechanical control coupled with sensorimotor learning enables AMOS to achieve more energy-efficient walking, compared to mere neuromechanical control [21]. The main contributions of the presented control and learning mechanisms are as follows:

- the developed muscle-like mechanisms (i.e., VAAMs) show a simple way to achieve variable compliant joint motions without complex sensory systems and (physical) compliant components;
- the integration of the VAAMs and a proximo-distal gradient leads a way to solve locomotor instabilities under active compliance control;
- the developed sensorimotor learning (see Fig. 1) presents a way to adaptive compliance control of a multi-legged robot with many DOFs;
- the neuromechanical control coupled with sensorimotor learning provides a way forward to model and control adaptive and energy-efficient legged locomotion with many DOFs.

II. Neuromechanical Controller Coupled with Sensorimotor Learning

A. Overview

We include the feed-forward and feedback pathways into our neuromechanical controller (see Fig. 1). For the feed-forward pathways, the controller not only consists of feed-forward control via descending commands (i.e., S, N_i, and O_i) from a neural circuit to muscle-like components and body mechanics, but also includes six forward models [38] for predicting force sensing (i.e., $F^p_{m,1}$) of the six legs. In the

[1]The cost of transport (i.e., COT) quantifies the energy efficiency transporting an animal or a vehicle from one place to another. It is also called specific tractive force or specific resistance.

feedback pathway, there is force sensing (i.e., $F^{ext}_{m,1}$) at the end effectors of the legs. Using $F^{p}_{m,1}$ and $F^{ext}_{m,1}$ as the inputs, 12 dual-rate learning processes can actively tune the stiffness parameters (i.e., K_j) of the muscle-like components driving 12 joints of the legs. This leads to variable compliant leg motions over different surfaces. Actively tuning mechanical properties (e.g., joint stiffness) is an important characteristic of animal locomotion [11], [39], [40], [41]. For example, the tunable mechanical properties of insect legs can help its locomotion over rough terrain [14], [42], [43].

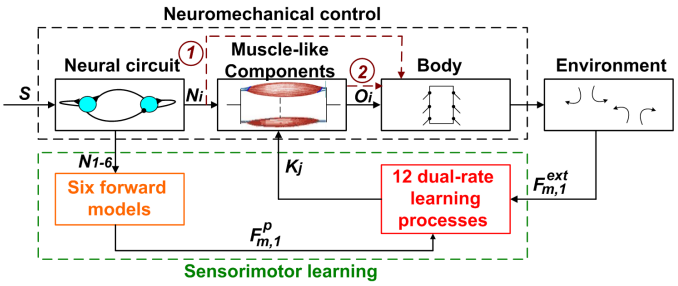

Fig. 1. Neuromechanical control coupled with sensorimotor learning applied to a hexapod robot AMOS. Via neural outputs N_i ($i = 1, 2, \ldots, 17, 18$), a neural circuit activates the muscle-like components that generate position commands (i.e., O_i) to move the leg joints of AMOS. The legs then interact with the environment, which produces force feedback (i.e., $F^{ext}_{m,1}$) ($m = 1, 2, \ldots, 5, 6$). Besides, six forward models predict expected force feedback (i.e., $F^{p}_{m,1}$) of the legs based on the outputs of the neural network. Using $F^{ext}_{m,1}$ and $F^{p}_{m,1}$ as the inputs, 12 dual-rate learning processes actively tune 12 stiffness parameters (i.e., K_j, $j = 7, 8, \ldots, 17, 18$) of muscle-like components driving 12 joints. There are three ways of generating position commands O_i driving the joints: feed-forward neural control for proximal joints (see ①), combining feed-forward neural control and tendon-like compliance for intermediate joints, and tendon-like compliance for distal joints (see ②). Interestingly, these three ways are comparable to a proximo-distal gradient [44], [45], [46] (see text for details).

In addition to neuromechanical interactions, studies of leg muscle architecture [47] and function [48], [49], [50] suggest that a proximo-distal gradient of muscle function and neural control exists, which reflects different control strategies for the joints [44], [45], [46], [51], [52]. Following the gradient, proximal joints are under feed-forward neural control, and are rarely sensitive to changes in loading during stance. By contrast, distal joints are more sensitive to loading, and are basically driven by tendons. This proximo-distal gradient enhances locomotor stability of legged animals on rough terrain [46], [53], [54]. Based on the gradient, the virtual agonist-antagonist mechanisms (i.e., VAAMs) emulate muscle-like mechanisms (see Fig. 1). The contractile (i.e., CEs) and passive (i.e., PEs) elements of the VAAMs implement feed-forward neural control [14] and compliance of tendons [55], respectively. The proximal joints (i.e., Thoraco Coxal joints) of the hexapod robot are driven by a neural circuit (see ① in Fig. 1) without muscle-like mechanisms (i.e., spring-damper mechanisms). Whereas its distal joints (i.e., Femur Tibia joints) are only actuated by the muscle-like mechanisms emulating the compliance of tendons (see ② in Fig. 1). The experimental results show that such a setup enables the hexapod robot to achieve more stable walking on rough surfaces (e.g., gravels). The setup enhances stability of legged robot locomotion under active compliance control which generally leads to locomotor instabilities [36], [37]. In the following, we describe three above introduced components of our system: (I) A neural circuit which produces the commands to coordinate joint motions and to change gaits based on energetic cost. (II) Biomechanical components consisting of muscle-like components and a bio-inspired body. Walking systems particularly require an adaptive muscle model where its parameters can be easily and quickly tuned to achieve proper compliant joint motions. (III) Sensorimotor learning which can predict sensory consequences of actions and actively tune compliance of joint motions; thereby enabling walking systems to accommodate different gaits and deal with different surfaces. The details of each component are described below.

B. Neural Circuit: Modular Neural Network (MNN)

Our modular neural network (MNN) is a biologically-inspired hierarchical neural controller [56], [57]. The MNN generates signals for inter- and intra-leg coordination of the six-legged robot AMOS. Each leg has a TC (Thoraco Coxal) joint allowing forward and backward motions, a CTr (Coxa Trochanteral) joint allowing elevation and depression motions, and an FTi (Femur Tibia) joint allowing extension and flexion motions. The MNN consists of a central pattern generator (CPG, see Fig. 2 (I)), a phase switch module (PSM, see Fig. 2 (II)) and two velocity regulating modules (VRMs, see Fig. 2 (III)). All neurons of the MNN are modeled as discrete-time, non-spiking neurons. The activation H_i of each neuron develops according to:

$$H_i(t) \quad = \quad \sum_{j=1}^{m} W_{ij}\, o_j(t-1) + B_i, \quad i = 1, \ldots, m, \quad (1)$$

where m denotes the number of units, B_i is an internal bias term (i.e., stationary input) to neuron i, W_{ij} is the synaptic strength of the connection from neuron j to neuron i. The output o_i of every neuron of the MNN is calculated using a hyperbolic tangent (tanh) transfer function, i.e., $o_i = \tanh(H_i), \in [-1, 1]$. The weights W_{ij} are manually designed, except weights a, b, and c which are obtained by back-propagation learning (see Fig.2 (III)). More details of determining the weights W_{ij}, we refer to our previous work [58].

The CPG consists of only two neurons with full connectivity [25] (see Fig. 2 (I)), where B_1 and B_2 are set to 0.01. The weights W_{12} and W_{21} are given by:

$$W_{12}(S) = 0.18 + S, W_{21}(S) = -0.18 - S, \quad (2)$$

where $S \in [0.01, 0.18]$ is the modulatory input determining the speed of the legs, which increases with increasing S.

The PSM is a generic feed-forward network consisting of three hierarchical layers with ten hidden neurons (i.e., $H_3 - H_{12}$) (see Fig. 2 (II)). The outputs of the PSM are projected to the FTi (i.e., $F(R, L)_{(1,2,3)}$) and CTr (i.e., $C(R, L)_{(1,2,3)}$) motor neurons (see Fig. 2 (IV)), as well as to the neurons H_{13} and H_{14} of the two VRMs (see Fig. 2 (III)). The VRMs are feed-forward networks projecting their outputs to the TC motor neurons $T(R, L)_{(1,2,3)}$ (see Fig. 2 (IV)). Delays λ_L and λ between the motor neurons are fixed (see Fig. 2 (IV)). The

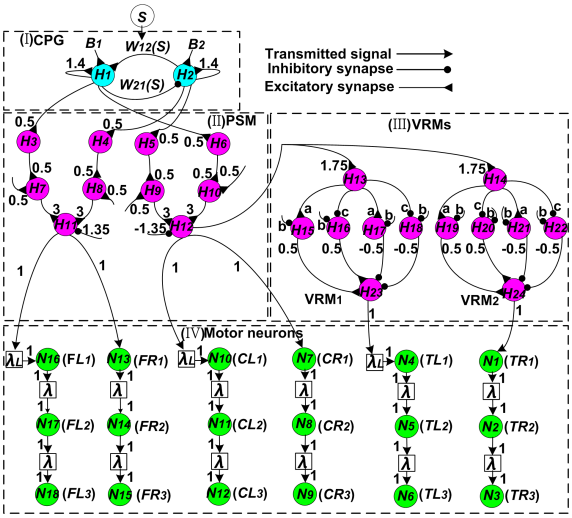

Fig. 2. Modular neural network. There are three different neuron groups: input neuron (S), hidden neurons (H_{1-24}) and output neurons (N_{1-18}). The input neuron is used to control walking patterns of the hexapod robot AMOS. The hidden neurons are divided into three modules: CPG, PSM and VRMs, which have different functionalities (see texts for details). The output neurons represent the neural activities of the joints of the robot. All connection strengths together with bias terms are indicated by the small numbers except some parameters of the VRMs ($a = 1.7246$, $b = -2.48285$, $c = -1.7246$). Delays λ_L and λ between output neurons are set to 48 time steps and 16 time steps, respectively. Abbreviations are: $TR(L)_{1,2,3}$ = TC joints of the Right(Left) Front, Middle, Hind legs, $CR(L)_{1,2,3}$ = CTr joints of the Right(Left) Front, Middle, Hind legs, $FR(L)_{1,2,3}$ = FTi joints of the Right(Left) Front, Middle, Hind legs. Abbreviations are: R(F, M, H) = Right (Front, Middle, Hind) leg, L(F, M, H) = Left (Front, Middle, Hind) leg.

outputs N_{1-18} of the motor neurons are the neural activities of the joints of the hexapod robot. Here, we show how N_{1-18} enable the legs to perform a fast wave gait [57] (see Fig.1 in supplementary information). In addition, nine gaits (see Fig.2 in supplementary information) are achieved by changing the modulatory input S (see Eq.(2)) of the modular neural network (MNN, see Fig.2). More details of the MNN can be seen at our previous work [58].

C. Biomechanical Components

1) Muscle-like Component - Virtual Agonist-antagonist Mechanism (VAAM): The virtual agonist-antagonist mechanism (VAAM) consists of a pair of agonist and antagonist mechanisms (see Fig. 3(a)). It produces active and passive forces using its contractile and parallel elements (CEs and PEs, see Fig. 3(b)). In Fig. 3(a), a physical joint is driven by a VAAM (i.e., $M1$ and $M2$). Virtual means that the joint, physically driven by a standard servo motor, imitates muscle-like behaviors as if it were driven by a pair of physical agonist and antagonist muscles. The joint actuation relies on the CEs, while the PEs govern joint compliance.

The parallel elements (i.e., PEs) are modeled as spring-damper systems (see Fig. 3(b)) in terms of a Voigt muscle model [59]. The active forces produced by the CEs are approximated by the product of the neural activity N_j and the activity strengths $i_{(1,2)}$. More details of mathematically modeling the PEs and CEs can be seen at our previous work [60]. We apply Euler's law to the rotation of the joint P (see

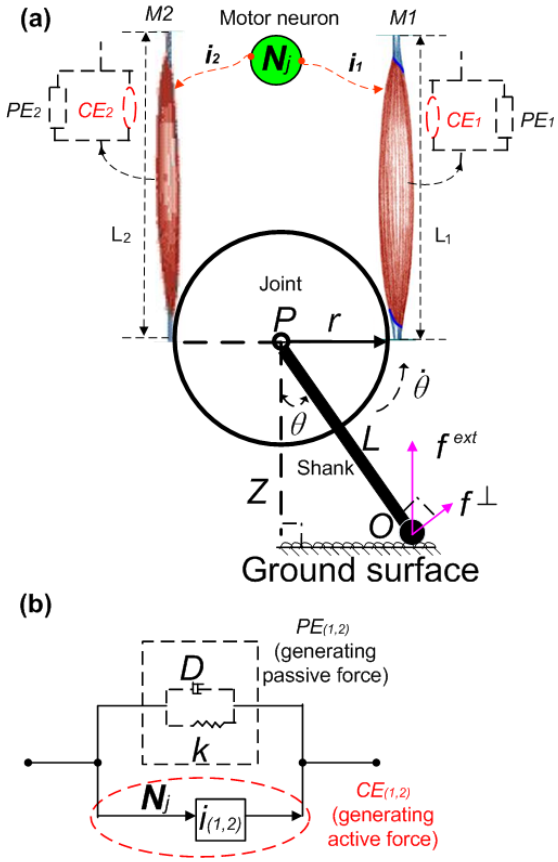

Fig. 3. Virtual agonist-antagonist mechanism (VAAM) for joint control interacting with the ground surface. (a) The physical joint P is driven by a VAAM (i.e., $M1$ and $M2$) with the lengths L_1 and L_2. The interaction results in an external force f^{ext}, which drives the joint P with radius r via the shank with length L. f^{ext} is sensed by a force sensor (i.e., O), and $f^{\perp}$ is the amount of f^{ext} directly perpendicular to the position of the joint P. θ is the rotational angle of the joint P relative to the absolute frame Z. (b) The agonist and antagonist mechanisms consist of contractile and parallel elements ($CE_{(1,2)}$ and $PE_{(1,2)}$). $PE_{(1,2)}$ are spring-damper systems producing passive forces. $CE_{(1,2)}$ generate active forces depending on the neural activity N_j and the activity strengths $i_{(1,2)}$ (i.e., $i_{(1,2)} \in [-1, 1]$). The neural activity N_j is one of the outputs N_{1-18} of the modular neural network (see Fig. 2 (IV)).

Fig. 3(a)). The motion equation of the joint P is given by:

$$I\ddot{\theta} = \underbrace{f^{ext}\sin(\theta)L}_{\text{torque by } f^{ext}} + [\underbrace{rN_j}_{\text{torque by } CE_{(1,2)}} \underbrace{-r(2K\theta r + 2D\dot{\theta}r)}_{\text{torque by } PE_{(1,2)}}]. \quad (3)$$

Equation (3) governs the angle θ of a physical joint driven by the VAAM that is activated by the output N_j ($j \in \mathbb{Z}_{[1,18]}$) of the MNN. The joint angle θ and joint velocity $\dot{\theta}$ in Eq.(3) are not from sensory feedback but calculated using fourth-order RungeKutta. In principle, this bio-inspired compliant joint control approach (i.e., the VAAM) shares a connection to classical impedance control approaches [61] in terms of spring-damper based compliance. However, it is a biological model where biological muscle functions (e.g., brakes [62]) can be easily emulated by changing stiffness and damper parameters (i.e., K and D in Eq.(3)) [63]. Here, through using sensorimotor learning (see section II-E for details), K will be adjusted in an online manner while D will keep fixed during walking. More advantages of the VAAM model are described

at our previous work [21].

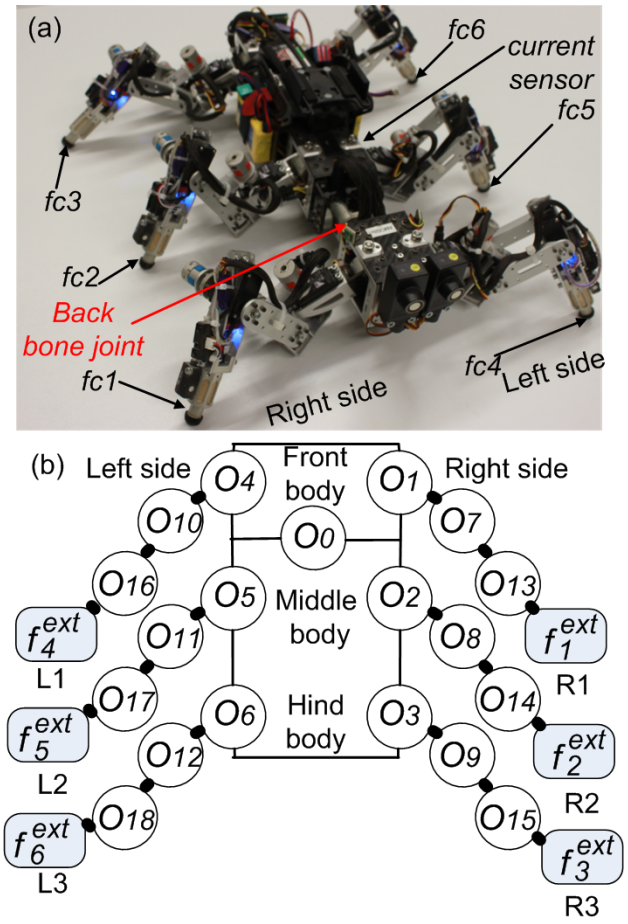

Fig. 4. Hexapod robot AMOS. Its three-jointed legs mimic leg morphology of an insect (see Figs.3 in supplementary information). (a) AMOS and its sensors. $fc_{(1-6)}$ are force sensors. (b) The outputs O_{0-18} controlling the 19 joints of AMOS when receiving analog signals f^{ext}_{1-6}, which are detected by the force sensors at the legs. Abbreviations are: L(1,2,3) = Left (Front, Middle, Hind) leg. R(1,2,3) = Right (Front, Middle, Hind) leg.

2) Bio-inspired Body - Hexapod Robot AMOS: Here we use a hexapod robot (i.e., AMOS, 5.4 kg weight, see Fig. 4 (a)) as our experimental platform. It has six three-jointed legs (see Figs.3 in supplementary information), and each leg emulates the morphology of a cockroach leg [64]. Every leg has a TC (Thoraco Coxal) joint allowing forward and backward motions, a CTr (Coxa Trochanteral) joint allowing elevation and depression motions, and an FTi (Femur Tibia) joint allowing extension and flexion motions (see Figs.3 in supplementary information). Each joint is physically driven by a standard servo motor (i.e., HSR-5990TG). There is a force sensor (i.e., FS Series Force Sensor) used for detecting an analog force signal at each leg (see fc_{1-6} in Fig. 4 (b)).

A current sensor, installed inside the body of the hexapod robot, is used to measure the electrical current supplied to all motors of the robot. Here, the current sensor signal is used to calculate power consumption during walking. The sensory data are transmitted via an RS232 serial connection to an external PC on which the controller is implemented. The final motor commands of the controller are sent to the robot also via the serial connection.

D. Neuromechanical Control: Combining Neural Circuit and Biomechanical Components

The outputs $O_{1-18} \in [-1, 1]$ of the neuromechanical controller are linearly scaled and transmitted to control the positions of the standard servo motors driving the 18 joints of the hexapod robot (see Fig.5 (b) in supplementary information). Note that the command O_0 here is set to a constant value (i.e., $O_0 = 0$) for controlling a backbone joint to the middle position. For joint control (i.e., O_{1-18}), different control strategies are applied to swing and stance phases, like virtual model controllers [65], [66].

1) Swing Phase: When a leg is in swing phases (i.e., f_i^{ext} = 0, $i = 1, 2, \ldots, 5, 6$), the motor neurons $N_{(i,i+6,i+12)}$ of the MNN (see Fig. 2 (IV)) are linearly transformed into the outputs $O_{(i,i+6,i+12)}$ controlling the TC, CTr, and FTi joints. $O_{(i,i+6,i+12)}$ satisfy:

$$[O_i, O_{i+6}, O_{i+12}]^T = [0.4N_i, 0.15N_{i+6}, -0.02N_{i+12}]^T - [0.05, -0.86, 0.43]^T, i \in \mathbb{Z}_{[1,6]}. \quad (4)$$

The details of Eq.(4) can be seen in Eqs.(A.(1-3)) of our previous work [21]. Note that the outputs $O_{(i,i+6,i+12)}$ are kept and transferred to the initial joint angles of the following stance phases. The keeping leads to smooth switches from swing to stance phases (see Fig.6 in supplementary information).

2) Stance Phase: The TC joint of the leg allowing only horizontal motion is not affected by the PEs of the VAAM since there is only detection of vertical foot force at the end effector of the leg. As a consequence, the TC joint is driven by the CEs of the VAAM that simulate feed-forward neural control. By contrast, the CTr and FTi joints, contributing to vertical motion of the leg, can be influenced by vertical foot force. Based on the VAAMs, we test nine possible setups (see Table I in supplementary information) to control the CTr and FTi joints in a physical simulator (i.e., lpzrobots simulator [67]). The simulation results show that the setup S2 is the best leading to coordinated movement and stable locomotion with the smallest body oscillation (see Fig.4 in supplementary information). The setup S2 is as follows: each TC joint (i.e., proximal joint) is purely controlled by the CEs of the VAAM (i.e., pure actuation), each CTr joint (i.e., intermediate joint) is governed by the CEs and PEs of the VAAM (i.e., combination of actuation and compliance), and each FTi joint (i.e., distal joint) is driven by the PEs (i.e., PE_1 and PE_2) of the VAAM (i.e., pure compliance) (see more details in Figs.5 of supplementary information). Interestingly, this setup also complies with a proximo-distal gradient revealed by biological studies on three-jointed leg locomotion [44], [52], [68]. These studies show that proximal joints mainly act as actuation while distal joints serve as compliance in legged animal locomotion. Such passive compliance and active actuation make the VAAM differ from virtual model control (VMC), which only contains a virtual passive element (e.g., spring) attached to the robot as if it had exited [65] (see Figs. 5). In contrast to VMC controllers [66], the VAAM not only includes the virtual passive elements (PEs) to act as muscle-like mechanisms, but also integrates the virtual contractile elements (CEs) to serve as neural control at the joints of legged robots. The

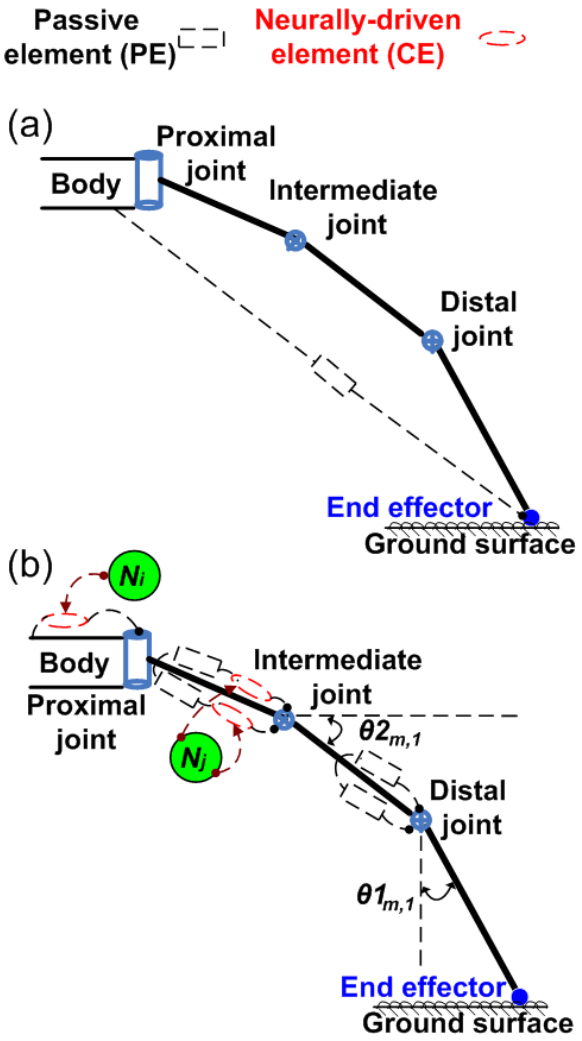

Fig. 5. Schematic diagrams of virtual model control (VMC) and VAAM control. (a) A virtual model controller [65] that only exploits a virtual passive element (e.g., spring) attaching the body to the end effector. (b) The VAAM controller that uses the virtual contractile and passive elements (i.e., CEs and PEs, see Figs. 3). The controller is based on the proximo-distal gradient (see more details in Figs.5 of supplementary information).

VAAM control is more bio-inspired control that generalizes the integration of neural control and muscle-like functions on coordinated and compliant control of legged robots, compared to VMC controllers. As a result, the VAAM control enables AMOS to not only achieve more stable walking under active compliance control (see Fig. 6), but also easily emulate muscle-like functions (e.g., brakes and springs) [63].

The outputs O_{1-18} of the proposed neuromechanical controller are calculated as follows:

All TC joints are purely controlled by $CE_{(1,2)}$ of the VAAM. The matrix of the outputs of the TC motor neurons is $T_{6\times1} = [N_1, N_2, \ldots, N_6]^T$ (see Fig. 2 (IV)). O_j are given by ($j \in \mathbb{Z}_{[1,6]}$):

$$O_j = 0.4T_{j,1} - 0.05. \quad (5)$$

The details of Eq.(5) can be seen in Eq.(A.4) of our previous work [21].

Each CTr joint is driven by $PE_{(1,2)}$ and $CE_{(1,2)}$ of the VAAM. The matrix $\theta 2_{6\times1}$ of the CTr angles is the sum of the Hadamard products (see Eqs.(17-18) as in our previous work [60]):

$$\begin{aligned} I\ddot{\theta 2}_{6\times1} &= F^{ext}_{6\times1} \circ (L_2 \cos(\theta 2_{6\times1}) + \vec{V}1_{6\times1}) \\ &\quad +[rC_{6\times1} - \\ &\quad 2r^2(K2_{6\times1} \circ \theta 2_{6\times1} + D2_{6\times1} \circ \dot{\theta 2}_{6\times1})]. \quad (6) \end{aligned}$$

The angles $\theta 2_{m,1}$ ($m \in \mathbb{Z}_{[1,6]}$, see $\theta 2_{6\times1}$ in Eq.(6)) of the CTr joints are linearly transformed into their outputs O_j (see more details in Figs.5 of supplementary information). O_j are given by ($j \in \mathbb{Z}_{[7,12]}$):

$$O_j = -0.8\theta 2_{m,1} - 0.38, m = j - 6. \quad (7)$$

The details of Eq.(7) can be seen in Eq.(A.5) of our previous work [21].

Each FTi joint is only driven by $PE_{(1,2)}$ of the VAAM (see more details in Figs.5 of supplementary information). The FTi angle matrix $\theta 1_{6\times1}$ is the sum of the Hadamard products (see Eqs.(13-15) as in our previous work [60]):

$$\begin{aligned} I\ddot{\theta 1}_{6\times1} &= F^{ext}_{6\times1} \circ \sin(\theta 1_{6\times1})L_1 - \\ &\quad 2r^2(K1_{6\times1} \circ \theta 1_{6\times1} + D1_{6\times1} \circ \dot{\theta 1}_{6\times1}). \quad (8) \end{aligned}$$

The angles $\theta 1_{m,1}$ ($m \in \mathbb{Z}_{[1,6]}$, see $\theta 1_{6\times1}$ in Eq.(8)) of the FTi joints can be linearly transformed into their outputs O_j (see more details in Figs.5 of supplementary information). O_j are given by ($j \in \mathbb{Z}_{[13,18]}$):

$$O_j = 0.92\theta 1_{m,1} + 0.12, m = j - 12. \quad (9)$$

The details of Eq.(9) can be seen in Eq.(A.6) of our previous work [21].

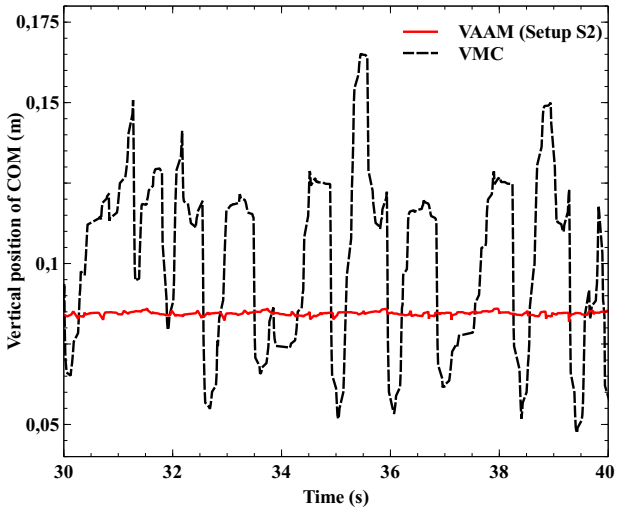

Fig. 6. Vertical positions of COM (Center Of Mass) of the hexapod robot AMOS. The experiments are conducted in the physical simulator lpzrobots [67]. The VAAM control (setup S2, see Table I in supplementary information) enables AMOS to walk stably (smaller body oscillation), compared to virtual model control (VMC).

E. Sensorimotor Learning for Adaptive Compliant Joint Motions

The adaptive compliant joint motions of AMOS are achieved by actively adjusting the stiffness parameters $K1_{6\times1}$

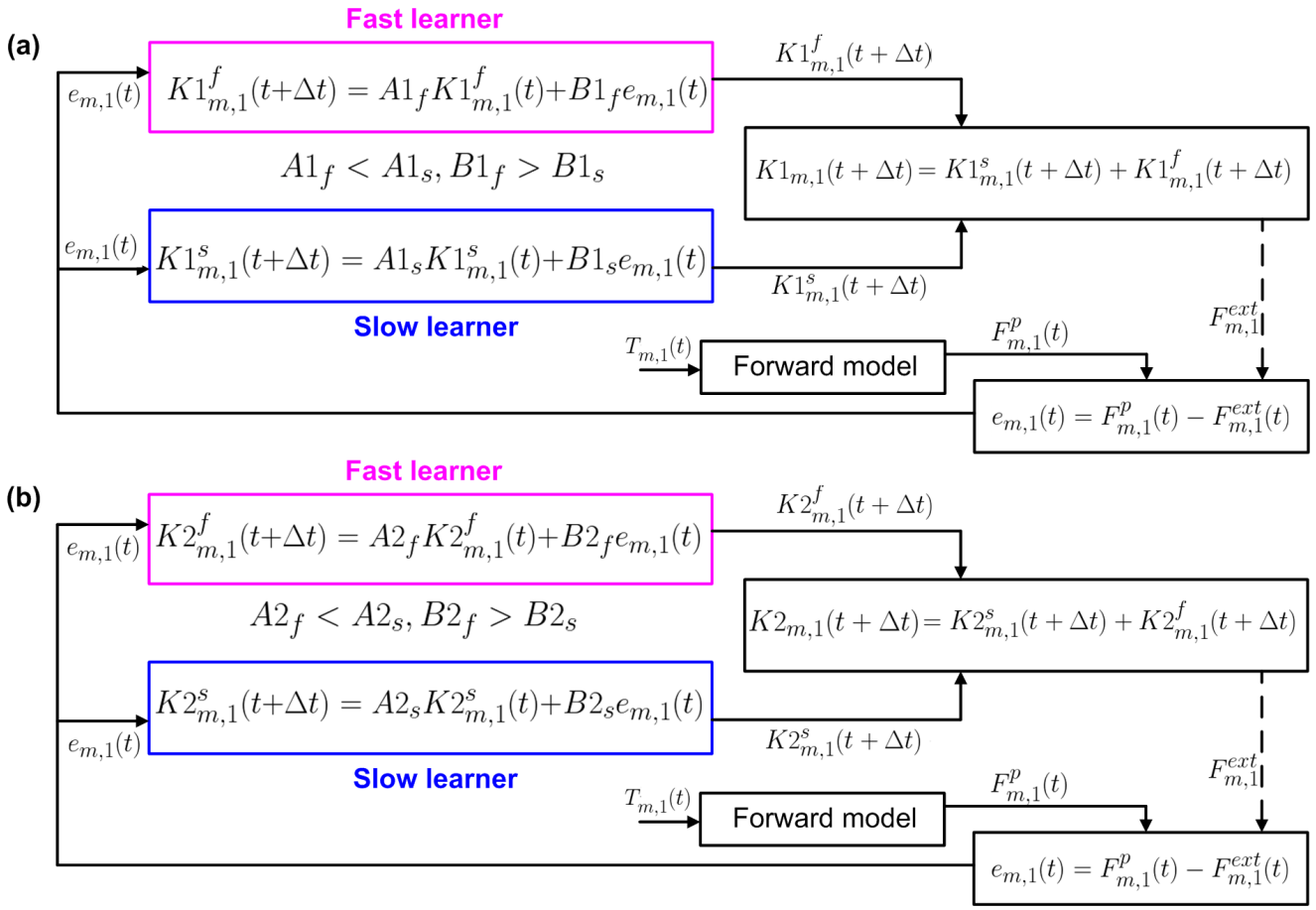

Fig. 7. Sensorimotor learning for stiffness parameters $K1_{m,1}$ and $K2_{m,1}$. $K1_{m,1}$ and $K2_{m,1}$ ($m = 1, 2, \ldots, 5, 6$) are stiffness parameters of the passive elements (i.e., PEs) driving the FTi and CTr joints of the AMOS's legs. For each leg, there are two dual-rate learning processes for adjusting stiffness parameters (e.g., $K1_{4,1}$ and $K2_{4,1}$) by using expected and real foot force signals (e.g., $F^p_{4,1}$ and $F^{ext}_{4,1}$). The expected foot force signal (e.g., $F^p_{4,1}$) is predicted by a forward model based on an output (e.g., O_4) driving the TC joint. Each dual-rate learning process consists of a fast learner and of a slower learner acting in parallel. (a) A dual-rate learning process for stiffness parameters $K1_{m,1}$. The parameters of the two learners are set as: $A1_f = 0.59$, $A1_s = 0.992$, $B1_f = 0.378$, and $B1_s = 0.036$. (b) A dual-rate learning for stiffness parameters $K2_{m,1}$. The parameters of the two learners are set as: $A2_f = 0.59$, $A2_s = 0.992$, $B2_f = 0.882$, and $B2_s = 0.084$.

and $K2_{6\times1}$ (see Eqs.(8) and (6)) of the passive elements (i.e., PEs) of the VAAMs driving the FTi and CTr joints. Here, we apply sensorimotor learning for online adjusting $K1_{6\times1}$ and $K2_{6\times1}$ at every time step Δt (i.e., $\Delta t = 0.019(s)$). For each leg, there are two dual-rate learning processes and a forward model (see Figs. 7 (a) and (b)) for the CTr and FTi joints. The forward model uses the outputs (i.e., $O_m(t)$) driving the TC joints to predict foot force signals (i.e., $F^p_{m,1}(t)$, $m = 1, 2, \ldots, 5, 6$). Specifically, $F^p_{m,1}(t)$ will gradually increase to 1 when $O_m(t)$ is decreasing (e.g., see $F^p_{4,1}(t)$ and $O_4(t)$ in Fig. 8 (a)). $F^p_{m,1}(t)$ are given by:

$$F^p_{m,1}(t+\Delta t) = 0.2G_{m,1}(t+\Delta t) + 0.8F^p_{m,1}(t),$$
$$G_{m,1}(t) = \begin{cases} 1, & O_m(t+\Delta t) < O_m(t). \\ 0, & O_m(t+\Delta t) > O_m(t). \end{cases} \quad (10)$$

The matrix $e_{6\times1}(t)$ of errors between expected and real foot force signals is:

$$e_{6\times1}(t) = F^{ext}_{6\times1}(t) - F^p_{6\times1}(t),$$
$$e_{6\times1}(t) = [e_1(t), e_2(t), \ldots, e_5(t), e_6(t)]^T, \quad (11)$$

where $F^{ext}_{6\times1}(t)$ is the matrix of the real foot force signals, i.e., $F^{ext}_{6\times1}(t) = f^{ext}_{1-6}(t)$ (see Figs.4). $F^p_{6\times1}(t)$ is the matrix of the predicted foot force signals, i.e., $F^p_{6\times1}(t) = f^p_{1-6}(t)$.

An error (e.g., $e_{4,1}(t)$) is used as the input to a dual-rate learning process. For reducing the error (e.g., see $e_{4,1}(t)$ at Fig.8 (b)), the process adjusts the stiffness parameter (e.g., $K1_{4,1}(t)$) of the PEs driving the FTi joint in each leg (see Fig. 7(a)). Each learning process consists of a fast learner and of a slow learner. Both learners are modeled as linear systems acting in parallel. The fast one learns compensating the error more quickly, is indicated by a higher learning rate, i.e., $B1_f > B1_s$. Whereas, the slow one retains previous states much better, is indicated by a high retention factor, i.e., $A1_f < A1_s$. Therefore, the matrix $K1_{6\times1}(t)$ of stiffness parameters for the FTi joints is given by:

$$K1^f_{6\times1}(t+\Delta t) = A1_f K1^f_{6\times1}(t) + B1_f e_{6\times1}(t),$$
$$K1^s_{6\times1}(t+\Delta t) = A1_s K1^s_{6\times1}(t) + B1_s e_{6\times1}(t),$$
$$K1_{6\times1}(t+\Delta t) = K1^f_{6\times1}(t+\Delta t) + K1^s_{6\times1}(t+\Delta t), \quad (12)$$

where $K1^f_{m,1}(t+\Delta t)$ are the outputs of fast learners, and

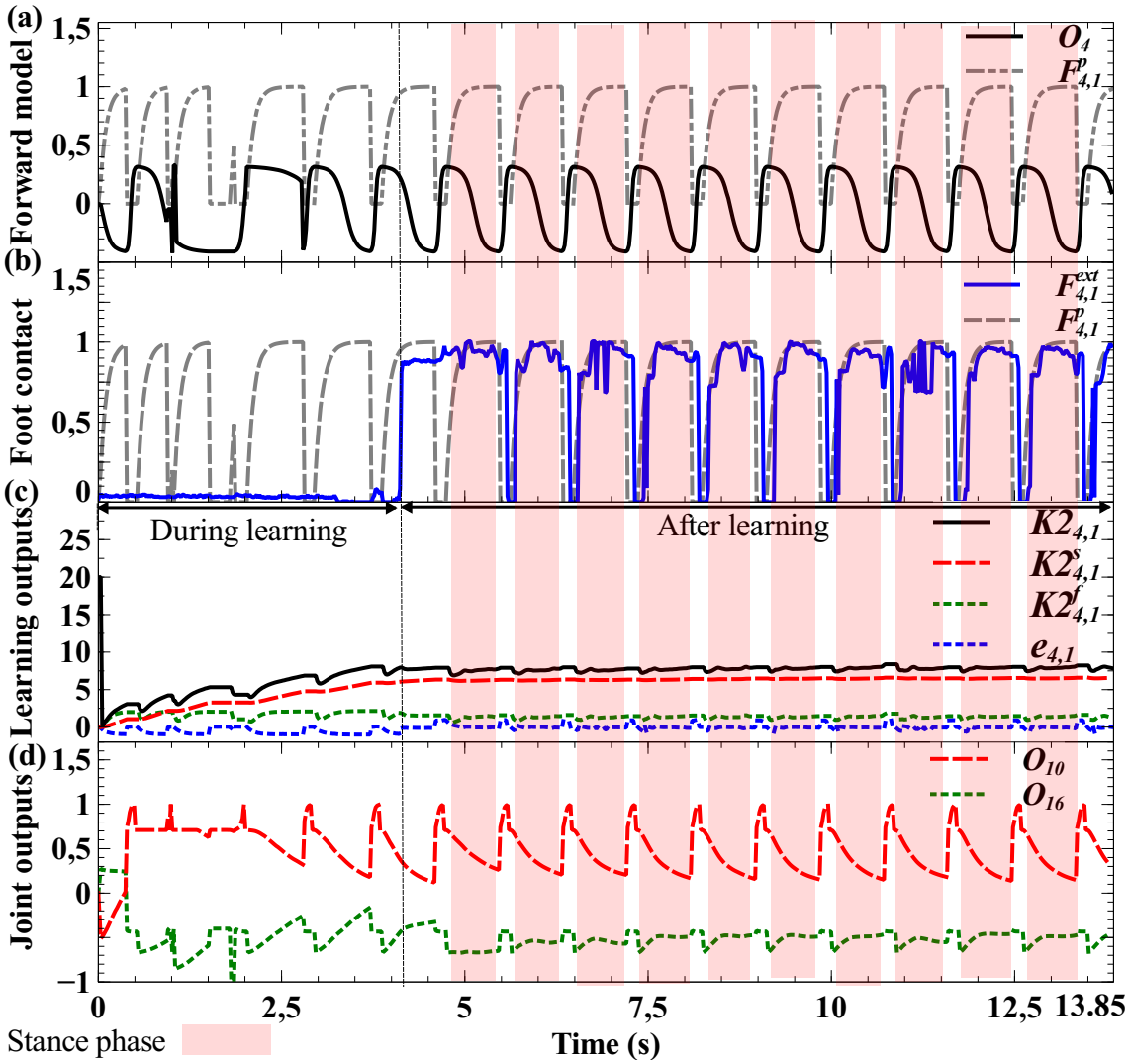

Fig. 8. Sensorimotor learning for adjusting stiffness parameter $K2_{4,1}$. Here the gait is fast caterpillar (i.e., the modulatory input $S = 0.10$). (a) Forward model. The output $O_4(t)$ driving the TC joint is applied to predict the foot force signal $F^p_{4,1}(t)$ (see Eq.(10)). (b) Contact forces. $F^{ext}_{4,1}(t)$ and $F^p_{4,1}$ are the real and predicted contact forces. (c) Learning the stiffness parameter $K2_{4,1}$. $K2_{4,1}$ is the sum of the outputs (i.e., $K2^f_{4,1}$ and $K2^s_{4,1}$) of a fast learner and a slow learner using the error $e_{4,1}$ between $F^{ext}_{4,1}$ and $F^p_{4,1}$ (see Eq.(13)). The adjustment of stiffness parameter $K1_{4,1}$ driving the FTi joint in the left front leg is shown in Fig.10 (a) (i.e., see LF). (d) O_{10}, and O_{16} are the outputs controlling the positions of the CTr and FTi joints in the left front leg.

$K1^s_{m,1}(t+\Delta t)$ are the outputs of slow learners. Note that the value of $A1_f$ and $A1_s$ are from [28], and $B1_f$ and $B1_s$ are empirically chosen (see all values in Fig. 7(a)).

Similarly, the matrix $K2_{6\times1}(t)$ of stiffness parameters (see Fig. 7(b)) for the CTr joints is given by:

$$\begin{aligned} K2^f_{6\times1}(t+\Delta t) &= A2_f K2^f_{6\times1}(t) + B2_f e_{6\times1}(t), \\ K2^s_{6\times1}(t+\Delta t) &= A2_s K2^s_{6\times1}(t) + B2_s e_{6\times1}(t), \\ K2_{6\times1}(t+\Delta t) &= K2^f_{6\times1}(t+\Delta t) + K2^s_{6\times1}(t+\Delta t), \end{aligned} \quad (13)$$

where $K2^f_{m,1}(t+\Delta t)$ are the outputs of fast learners, and $K2^s_{m,1}(t+\Delta t)$ are the outputs of slow learners. Note that the value of $A2_f$ and $A2_s$ are from [28], and $B2_f$ and $B2_s$ are empirically chosen (see all values in Fig. 7(b)). The Eqs.(12) and (13) are written in terms of time t different from the equations in [28] and [29] formulated according to trial number n.

III. Experiments

A. Sensorimotor Learning for Self-Adjusting Stiffness Parameters

For each leg, there are two learning processes coupled with a forward model (see Fig. 7) for adjusting the stiffness parameters (e.g., $K1_{4,1}$ and $K2_{4,1}$). At the left front leg, for example, there are two outputs (i.e., $K2^f_{4,1}$ and $K2^s_{4,1}$) of a fast learner and a slow learner acting in parallel, which contribute to stiffness parameter $K2_{4,1}$ (see Fig.8 (c)). One can see that the fast one learns $K2^f_{4,1}$ more rapidly, which leads to smaller oscillations (see green dashed line in Fig. 8 (c)). By contrast, the slow one retains $K2^s_{4,1}$ better, thereby leading to the convergence (see red dashed line in Fig. 8 (c)). This is because the retention factor $A2_f = 0.59$ of the fast learner is lower than $A2_s = 0.992$ of the slow learner (see Eq.(13)). Moreover, the fast learner is more sensitive to the

perturbations (i.e., stance phases) after learning (see Fig. 9), compared to the slow learner. This is because the learning rate $B2_f = 0.882$ of the fast learner is higher than $B2_s = 0.084$ of the slow learner (see Eq.(13)). The combination of the slow and fast learners enables the stiffness parameters (e.g., $K2_{4,1}$) to achieve global convergences and local oscillatory stiffness responds (see Figs. 8 (c) and 9), which lead to stable and adaptive compliant hexapedal walking on challenging surfaces. Furthermore, the stiffness parameters (e.g., $K2_{4,1}$) during swing phases are higher than them during stance phases (see Fig. 9), since they (during the swing phases) are kept as the stiffness parameters from the previous stance phases. Note that sensorimotor learning (see Eqs. (10)-(13)) is not applied to adaptively control the joints during swing phases, since there is only feed-forward neural control (see Eq.(4)) on the joints during swing phases. Whereas during stance phases, the stiffness parameters (e.g., $K2_{4,1}$) initially decrease and increase afterwards (e.g., see Fig. 9). This is because the muscle-like mechanisms (i.e., VAAMs) need to initially soften the joints to absorb impacts of external loads, and afterwards stiffen them to obtain more forces to move forward. Similarly, the PEs of the VAAMs also soften and stiffen the FTi joints during stances phases (see Fig. 10 (a)). In other words, the VAAMs stiffen when the external load increases (i.e., stance phases). This property of the VAAMs is comparable to that of biological muscles, which become stiff when the external load increases [69], [10]. The video of the experiment can be seen at http://www.youtube.com/watch?v=B0v5D9yiRH4. Note that AMOS had difficulties to walk on all experimental surfaces when only fast or slow learners were used to tune stiffness parameters $K1_{6\times1}$ and $K2_{6\times1}$. The video of the experiment can be seen at http://www.youtube.com/watch?v=Lq22FibYLE4. This is because the slow or fast learners allow only for global convergences or local oscillatory stiffness responds (see Fig. 9). Whereas combining the slow and fast learners, the dual-rate learners enable $K1_{m,1}$ and $K2_{m,1}$ to achieve global convergences (see Fig. 8 (c)) and local oscillatory stiffness responds (see Figs. 10), thereby leading to stable and adaptive walking on different surfaces. Moreover, the ranges of the stiffness parameters $K1_{m,1}$ and $K2_{m,1}$ vary between hind and non-hind legs. Lower $K1_{(3,6),1}$ and higher $K2_{(3,6),1}$ (see LH and RH in Figs. 10) press the hind legs more down, which enhance locomotion stability, compared to the front and middle legs. This is because the mass of AMOS mainly concentrates on its hind part. Furthermore, the values of $B(1,2)_f$ and $B(1,2)_s$ are empirically chosen to produce proper stiffness parameters $K1_{m,1}$ and $K2_{m,1}$ (see Figs. 7), which leads to appropriate (e.g., smooth) compliant joint motions of AMOS. For example, the compliant CTr joint motions are more smooth (see $K2_{m,1} = 9.0$ in Fig. 11) when the parameters $K2_{m,1}$ of their driving VAAMs are self-adjusted between 6.5 and 13.5 (see Fig. 10 (b)).

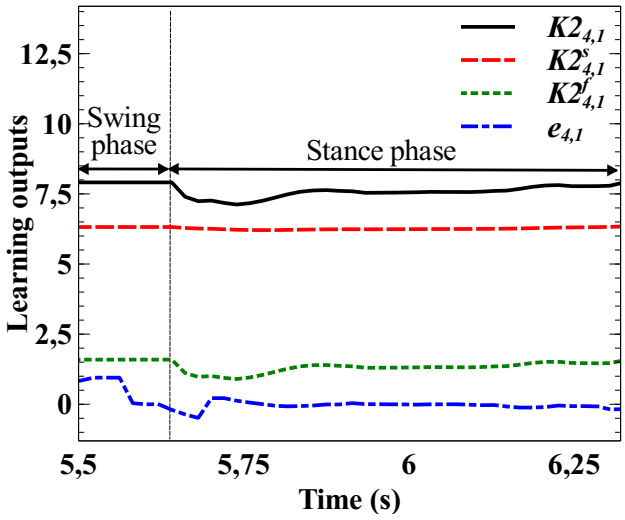

Fig. 9. Sensorimotor learning for adjusting stiffness parameter $K2_{4,1}$ during a swing and stance phases (see more details at Figs. 8). The figure is clipped from Fig. 8 (c).

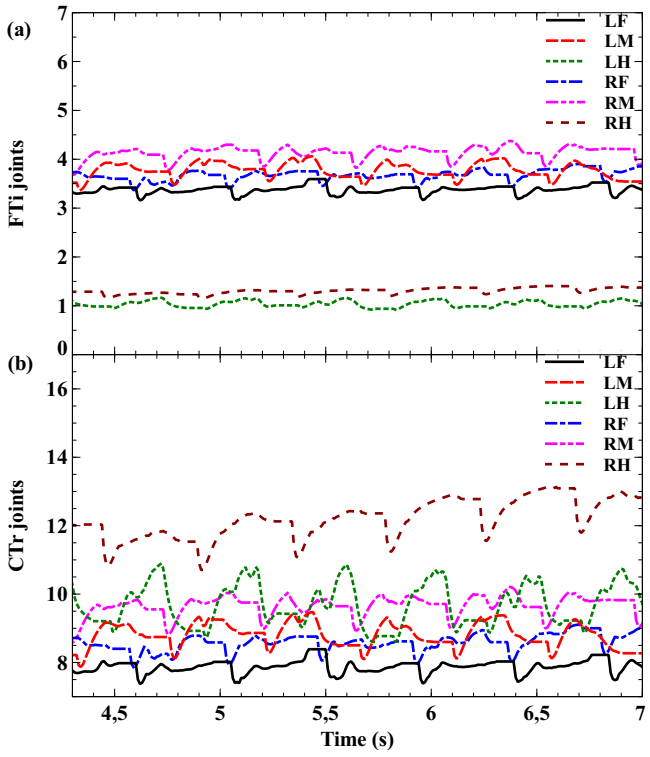

Fig. 10. Stiffness parameters $K1_{m,1}$ and $K2_{m,1}$ after learning. $m = 1, 2, \ldots, 5, 6$. The figure is clipped from Fig. 8 (c). Abbreviations are: R(F, M, H) = $K1_{(1,2,3),1}$, L(F, M, H) = $K1_{(4,5,6),1}$. (b) Stiffness parameters $K2_{m,1}$ for the CTr joints. The compliances of CTr joint motions are determined by the stiffness parameters $K2_{m,1}$ (see Eqs.(6)). Abbreviations are: R(F, M, H) = $K2_{(1,2,3),1}$, L(F, M, H) = $K2_{(4,5,6),1}$.

B. Adaptive Leg Compliance for Different Gaits

Actively tuning stiffness parameters $K1_{6\times1}$ and $K2_{6\times1}$ allows AMOS to accommodate different gaits. AMOS, for instance, walked on fine gravel when slow wave (i.e., $S = 0.02$) and fast caterpillar (i.e., $S = 0.10$) gaits were chosen (see Figs.2 (a) and (e) in supplementary information), respectively. One can see that AMOS softens and stiffens its CTr and FTi joints during stance phases, no matter which gait is chosen (e.g., see the gray area in Figs. 12

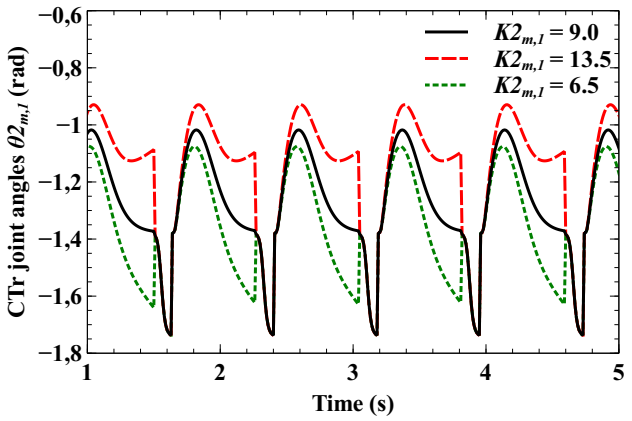

Fig. 11. The smoothness of the compliant CTr joint motions that varies with the stiffness parameters $K2_{m,1}$. Note that changing initial joint angles $\theta 2_{m,1}$ doesn't affect the smoothness of the compliant CTr joint motions (see Fig. 6 in supplementary information).

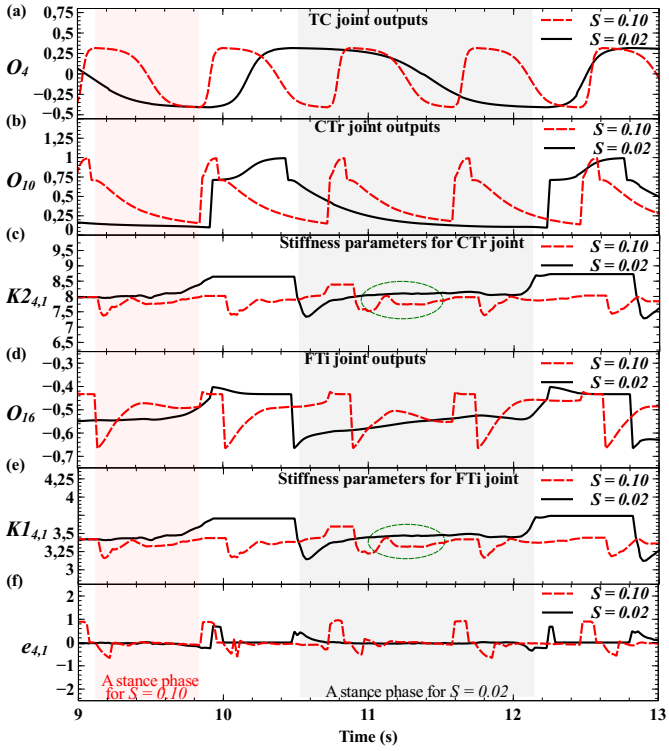

Fig. 12. Adjustments of $K1_{4,1}$ and $K2_{4,1}$ for different gaits. AMOS walked on fine gravel where its gait was chosen as slow wave (i.e., $S = 0.02$) and fast caterpillar (i.e., $S = 0.10$) gait, respectively. Sensorimotor learning enables AMOS to self-adjust stiffness parameters $K1_{4,1}$ and $K2_{4,1}$ for the left front leg. (a) TC joint outputs O_4. (b) CTr joint outputs O_{10}. (c) Stiffness parameters $K2_{4,1}$ determine the compliance of CTr joint motions of the left front leg. (d) FTi joint outputs O_{16}. (e) Stiffness parameters $K1_{4,1}$ determine the compliance of FTi joint motions of the left front leg. (f) Foot contact force errors $e_{4,1}$.

(c) and (e)). The video of the experiments can be seen at http://www.youtube.com/watch?v=tmqr65qIOTY . Moreover, the slow wave gait enables CTr and FTi joints to achieve stiffer motions that result from larger $K1_{m,1}$ and $K2_{m,1}$ (e.g., see green dashed circles in Figs. 12 (c) and (e)), compared to the fast caterpillar gait. That is, AMOS stiffens the legs during stance phases when the speed of its leg motion is reduced from the fast gait to the slow gait. This result is comparable to the finding of physiological experiments, which had shown that at low speed animals walk by vaulting stiffer legs [70], [24]. By contrast, AMOS softens its legs when the speed of its leg motion is increased from the slow gait to the fast one. This finding may reflect a control strategy of polyped (i.e., $>$ two legs) locomotion where polyped systems soften the legs owing to energy efficiency requirements [3]. Our experimental results also show that the fast caterpillar gait (i.e., $S = 0.10$) allows AMOS to achieve softer leg motions which lead to more energy-efficient locomotion on all experimental surfaces (see Costs of transport in Figs. 14), compared to the slow wave gait (i.e., $S = 0.02$).

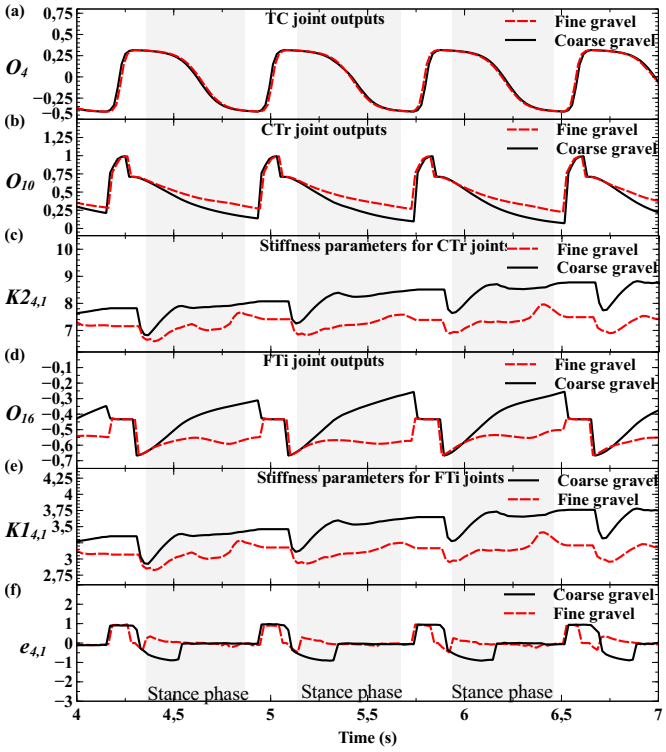

Fig. 13. Adjustments of $K1_{4,1}$ and $K2_{4,1}$ for different surfaces. An intermixed gait (i.e., modulatory input $S = 0.12$) was chosen for AMOS to walk on fine and coarse gravel, respectively. Sensorimotor learning enables AMOS to self-adjust stiffness parameters $K1_{4,1}$ and $K2_{4,1}$ for the left front leg. (a) TC joint outputs O_4. (b) CTr joint outputs O_{10}. (c) Stiffness parameters $K2_{4,1}$ determine the compliance of the CTr joint motions of the left front leg. (d) FTi joint outputs O_{16}. (e) Stiffness parameters $K1_{4,1}$ determine the compliance of the FTi joint motions of the left front leg. (f) Foot contact force errors $e_{4,1}$.

C. Adaptive Leg Compliance for Walking on Different Surfaces

Actively changing stiffness parameters $K1_{6\times1}$ and $K2_{6\times1}$ also leads to adaptive locomotion on different surfaces, for example, when an intermixed gait (i.e., modulatory input $S = 0.12$) was chosen for AMOS to walk on fine and coarse gravel, respectively. On these two surfaces, AMOS

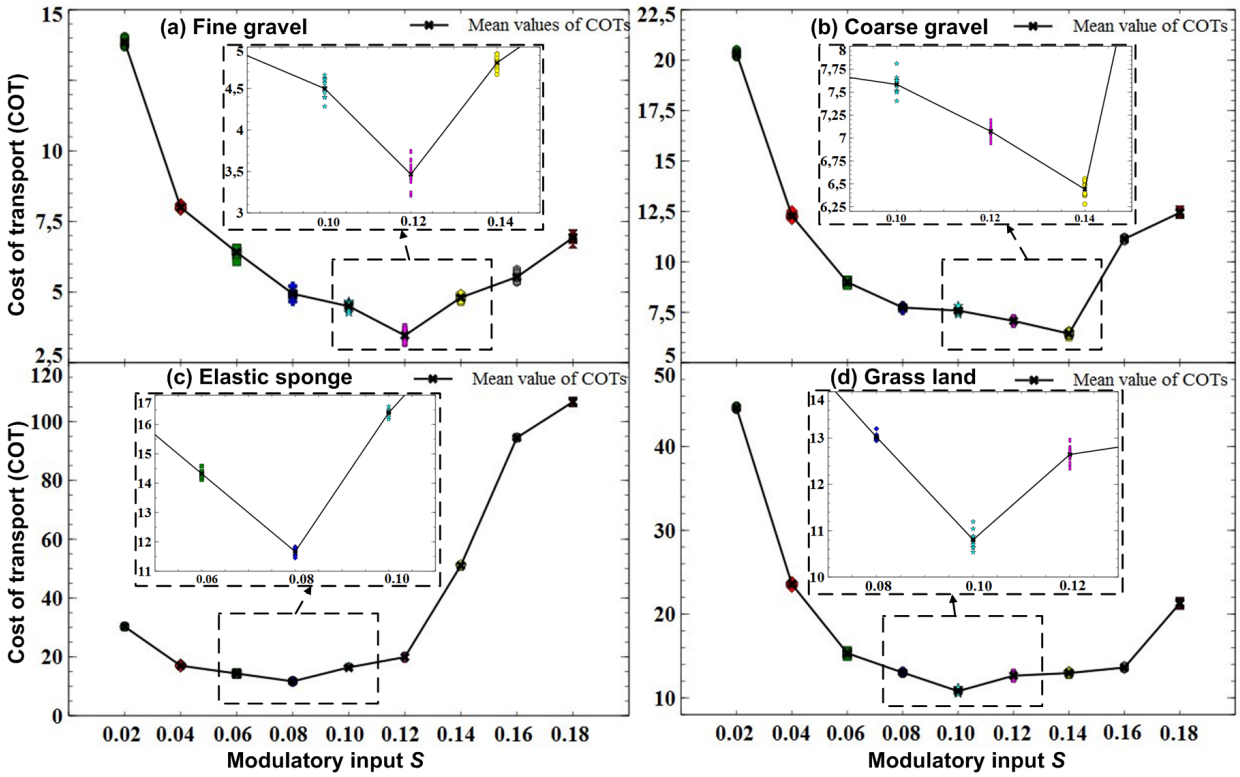

Fig. 14. Energy efficiencies of AMOS walking on different surfaces using different gaits. The energy efficiency is measured by cost of transport COT (i.e., specific resistances, see Eq.(14)). Lower COT corresponds to more energy efficient locomotion. Nine gaits (see Figs.2 in supplementary information) were chosen for AMOS walking over each experimental surface. (a) COTs on fine gravel. The slow intermixed gait (i.e., $S = 0.12$) enables AMOS to achieve more energy efficient walking. (b) COTs on coarse gravel. The Fast intermixed gait (i.e., $S = 0.14$) is more energy-efficient for its walking on this surface. (c) COTs on elastic sponge. The slow caterpillar gait (i.e., $S = 0.08$) is the optimizer gait. (d) COTs on grass land. The fast caterpillar gait (i.e., $S = 0.10$) allows AMOS to achieve more energy efficient walking.

joints receive the same motor neuron outputs[2] of the modular neural network (i.e., MNN, see Fig. 2). One can see that the TC joint motions of the left front leg are the same (see Fig. 13 (a)) because they are controlled by only feed-forward neural control (i.e., without passive elements). By contrast, CTr and FTi joint motions are different (see Figs. 13 (b) and (d)) during stance phases when AMOS walks on fine and coarse gravel, respectively. This is because TC, CTr, and FTi joints act with different roles (i.e., compliance or actuation, see more details in Figs.5 of supplementary information) for controlling leg motions in stance phases. Moreover, we can see that the CTr and FTi joints are stiffer[3] (i.e., higher $K1_{4,1}$ and $K2_{4,1}$ values, see Figs. 13 (c) and (e)) when AMOS walked on coarse gravel, compared to fine gravel. This makes the legs penetrate more deeply, but also extend more widely into the coarse gravel (see CTr and FTi joint motions in Figs. 13 (b) and (d)). The video of the experiments can be seen at http://www.youtube.com/watch?v=-Du62APFUt0 .

[2]In our work, the same modulatory input S of the modular neural network (i.e., MNN) corresponds to same motor neuron outputs (i.e., N_{1-18} in Fig. 2(IV)).

[3]A joint greatly resists the influence of external forces, and is thus "stiff". Whereas, a joint allows external forces to influence its movement easily, and is thus "soft" [71].

D. Energy Efficient Walking

In the previous subsections, we show that the proposed neuromechanical controller coupled with sensorimotor learning enables AMOS to produce coordinated and variable compliant joint motions that accommodate different gaits and surfaces. For each surface, nine gaits (see Figs.2 in supplementary information) are chosen by changing the modulatory input S (see Eq.(2)) of the modular neural network (MNN, see Fig.2). The variable compliant joint motions lead to different energy efficiencies of AMOS walking on fine gravel, coarse gravel, elastic sponge (stiffness 0.523 kN/m), and grass land. Typically, the energy efficiency is measured by cost of transport COT (i.e., specific resistance [30], [18]) as:

$$COT = \frac{P_{avg}}{mgv_{avg}}, v_{avg} = \frac{d}{t} \tag{14}$$

where P_{avg} is average power consumption. mg is the weight of AMOS, i.e., mg = 52.974 N. v_{avg} is its average forward speed when AMOS walks a distance d using time t. For each gait, we repeatedly ran the hexapod robot on each surface until ten successful runs were obtained. For each successful run, the average power consumption P_{avg} was calculated based on the electrical current supplied to all motors of AMOS, which is measured by a current sensor. Low COT corresponds to more energy efficient walking.

Figures 14 show costs of transport (i.e., COTs) when AMOS

TABLE I
THE COMPARISON BETWEEN THE HEXAPOD ROBOTS

Hexapod robots	AMOS	RHex [18]	Gregor I [72]
COTs	$3.4-11.7$	$3.7-14$	70
DOFs	19	6	16

walked on the four surfaces using the nine gaits. One can see that AMOS achieves more energy efficient walking by using gaits with intermediate leg speeds, compared to a slower leg speed (i.e., modulatory input $S = 0.02$, slow wave gait) or a faster leg speed (i.e., $S = 0.18$, fast tripod gait). Moreover, different gaits let AMOS consume different energetic costs. For instance, the slow intermixed gait (i.e., $S = 0.12$) enables AMOS to achieve more energy efficient walking on fine gravel (see Fig. 14 (a)) while the fast intermixed gait (i.e., $S = 0.14$) is an efficient gait for AMOS walking on coarse gravel (see Fig. 14 (b)). The slow (i.e., $S = 0.08$) and fast (i.e., $S = 0.10$) caterpillar gaits make AMOS achieve more energy efficient walking on elastic sponge and grass land, respectively (see Figs. 14 (c) and (d)). The video of the experiments can be seen at http://www.youtube.com/watch?v=SrasTYQG8Xk . Integrating neuromechanical control and sensorimotor learning, the adaptive neuromechanical controller (see Fig. 1) enables AMOS to achieve adaptive compliant walking, which effectively accommodates different gaits and surfaces. Such walking is achieved by online adjusting stiffness parameters $K1_{6\times1}$ and $K2_{6\times1}$ (see Eqs.(12) and (13)) of the passive elements (i.e., PEs) driving the FTi and CTr joints. Note that all damper parameters $D(1,2)_{m,1}$ (see Eqs.(8) and (6)) are set to 1.0 in all experiments chosen by trial and error. As a result, the adaptive neuromechanical controller (see Fig. 1) reduces COT of AMOS's walking to between 3.4 and 11.7, compared to our previous work [21]. Similarly, the adaptive neuromechanical controller allows for lower COT that corresponds to more energy-efficient walking (see Fig. 15 (a)), compared to the adaptive neural controller [22]. This is because the adjustable VAAMs of the adaptive neuromechanical controller result in compliant and smooth joint outputs (e.g., see Fig. 15 (b)), which lead to proper (e.g., deeper) leg penetrations into challenging surfaces (e.g., coarse gravel). Whereas other neural controllers [58] like the adaptive neural controller [22] cannot achieve such leg penetrations due to the lack of the muscle-like mechanisms (e.g., VAAMs). Moreover, the adaptive neuromechanical controller makes AMOS achieve more energy-efficient walking (see Table I and Figs.7 in supplementary information), compared to other small legged robots (less than 8 kg [31]).

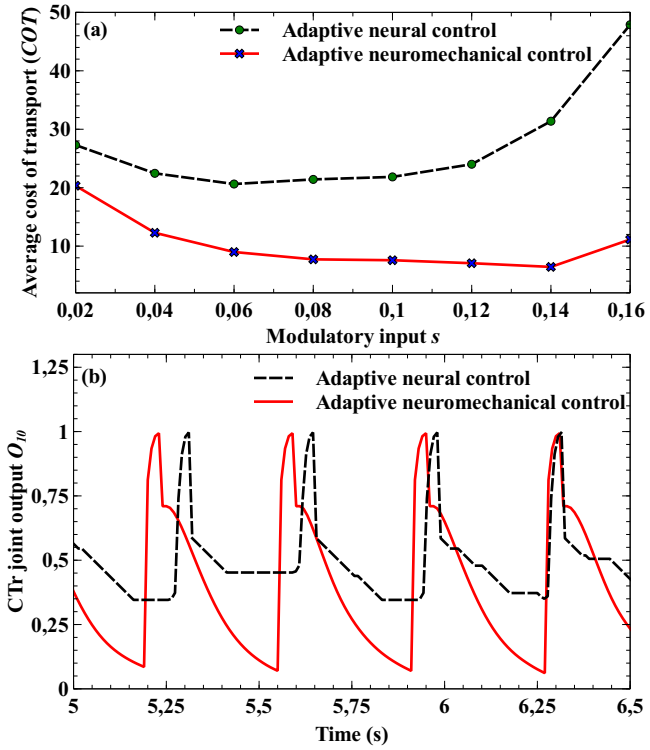

Fig. 15. Costs of transports COT and CTr joint outputs under the adaptive neuromechanical (see Fig. 1) and neural [22] controllers. The experimental surface is coarse gravel. (a) Costs of transports COT. (b) CTr joint outputs O_{10} (with fast intermixed gaits, modulatory input $S = 0.14$).

IV. Discussion and Conclusion

The proposed method (see Fig. 1) enables our legged robot to achieve variable compliant joint motions with self-adjustments that accommodate different gaits and surfaces. These motions are generated by online tuning 12 stiffness parameters (i.e., $K1_{m,1}$ and $K2_{m,1}$, $m = 1, 2, \ldots, 5, 6$) of the muscle-like mechanisms (i.e., the VAAMs) driving 12 joints. This online tuning is achieved by sensorimotor learning (see Fig. 1) with only force feedback at the end effectors of the legs. It is distinct from variable active compliance which is achieved by using force/torque feedback at each joint of the legs [33]. Moreover, active compliance control often gives rise to unstable locomotion on tough terrain (e.g., see VMC in Fig. 6)[37], [36]. Whereas our method utilizes the proximo-distal gradient to enhance locomotor stability on tough terrain (e.g., gravels) (see Fig.4 in supplementary information). Our method also differs from passive compliance, which is characterized by physical passive components (e.g., springs and dampers [73]) [74]. In addition, the proposed VAAM is a computational muscle model which can be easily applied to control physical legged robots [21], [63]. Thereby, the VAAM is also different from the Hill muscle model [26], [27] where there are typically 26 parameters to be tuned, usually used in computer simulations [75]. In conclusion, the main contribution of the work introduced here is that we present a way forward to understand and solve Bernstein's problem [15] of how to efficiently control many degrees of freedom in multi-legged locomotion tasks. This allows our legged robot to achieve adaptive and energy efficient walking without complex passive components or force/torque sensing systems.

References

[1] D. P. Ferris, M. Louie, and C. T. Farley, "Running in the real world: adjusting leg stiffness for different surfaces," *Proceedings of the Royal Society of London. Series B: Biological Sciences*, vol. 265, no. 1400, pp. 989–994, 1998.

[2] C. T. Farley, H. H. P. Houdijk, C. Van Strien, and M. Louie, "Mechanism of leg stiffness adjustment for hopping on surfaces of different

stiffnesses," *Journal of Applied Physiology*, vol. 85, no. 3, pp. 1044–1055, 1998.

[3] A. J. Spence, "Control strategies for legged locomotion: a comparative approach," in *7th European Nonlinear Dynamics Conference (ENOC), Rome, Italy.*, 2011.

[4] A. E. Kerdok, A. A. Biewener, T. A. McMahon, P. G. Weyand, and H. M. Herr, "Energetics and mechanics of human running on surfaces of different stiffnesses," *Journal of Applied Physiology*, vol. 92, no. 2, pp. 469–478, 2002.

[5] R. Full, C. Farley, and J. Winters, "Musculoskeletal dynamics in rhythmic systems: A comparative approach to legged locomotion," in *Biomechanics and Neural Control of Posture and Movement*, J. Winters and P. Crago, Eds. Springer New York, 2000, pp. 192–205.

[6] T. A. McMahon and G. C. Cheng, "The mechanics of running: How does stiffness couple with speed?" *Journal of Biomechanics*, vol. 23, Supplement 1, no. 0, pp. 65 – 78, 1990, international Society of Biomechanics.

[7] J. Nishii, "Legged insects select the optimal locomotor pattern based on the energetic cost," *Biological Cybernetics*, vol. 83, no. 5, pp. 435–442, 2000.

[8] J. Nishi, "Gait pattern and energetic cost in hexapods," in *Engineering in Medicine and Biology Society, 1998. Proceedings of the 20th Annual International Conference of the IEEE*, vol. 5, Oct 1998, pp. 2430–2433 vol.5.

[9] L. A. Miller, D. I. Goldman, T. L. Hedrick, E. D. Tytell, Z. J. Wang, J. Yen, and S. Alben, "Using computational and mechanical models to study animal locomotion," *Integrative and Comparative Biology*, vol. 52, no. 5, pp. 553–575, 2012.

[10] K. Nishikawa, A. A. Biewener, P. Aerts, A. N. Ahn, H. J. Chiel, M. A. Daley, T. L. Daniel, R. J. Full, M. E. Hale, T. L. Hedrick, A. K. Lappin, T. R. Nichols, R. D. Quinn, R. A. Satterlie, and B. Szymik, "Neuromechanics: an integrative approach for understanding motor control," *Integrative and Comparative Biology*, vol. 47, no. 1, pp. 16–54, 2007.

[11] E. Tytell, P. Holmes, and A. Cohen, "Spikes alone do not behavior make: why neuroscience needs biomechanics," *Current Opinion in Neurobiology*, vol. 21, no. 5, pp. 816 – 822, 2011, networks, circuits and computation.

[12] J. Abbas and R. Full, "Neuromechanical interaction in cyclic movements," in *Biomechanics and Neural Control of Posture and Movement*, J. Winters and P. Crago, Eds. Springer New York, 2000, pp. 177–191.

[13] H. J. Chiel, L. H. Ting, Ö. Ekeberg, and M. J. Z. Hartmann, "The brain in its body : Motor control and sensing in a biomechanical context," *Journal of Neuroscience*, vol. 29, no. 41, pp. 12 807–12 814, 2009, qC 20100525.

[14] S. Sponberg and R. J. Full, "Neuromechanical response of musculoskeletal structures in cockroaches during rapid running on rough terrain," *Journal of Experimental Biology*, vol. 211, no. 3, pp. 433–446, 2008.

[15] N. Bernstein, *The coordination and regulation of movements*. Oxford : Pergamon Press, 1967.

[16] R. Full and A. Ahn, "Static forces and moments generated in the insect leg: comparison of a three-dimensional musculo-skeletal computer model with experimental measurements," *The Journal of Experimental Biology*, vol. 198, no. 6, pp. 1285–1298, 1995.

[17] R. Full and D. Koditschek, "Templates and anchors: neuromechanical hypotheses of legged locomotion on land," *Journal of Experimental Biology*, vol. 202, no. 23, pp. 3325–3332, 1999.

[18] U. Saranli, M. Buehler, and D. E. Koditschek, "Rhex: A simple and highly mobile hexapod robot," *The International Journal of Robotics Research*, vol. 20, no. 7, pp. 616–631, 2001.

[19] K. Galloway, J. Clark, M. Yim, and D. Koditschek, "Experimental investigations into the role of passive variable compliant legs for dynamic robotic locomotion," in *Robotics and Automation (ICRA), 2011 IEEE International Conference on*, may 2011, pp. 1243 –1249.

[20] D. E. Koditschek, R. J. Full, and M. Buehler, "Mechanical aspects of legged locomotion control," *Arthropod Structure & Development*, vol. 33, no. 3, pp. 251 – 272, 2004, arthropod Locomotion Systems: from Biological Materials and Systems to Robotics.

[21] X. Xiong, F. Wörgötter, and P. Manoonpong, "Neuromechanical control for hexapedal robot walking on challenging surfaces and surface classification," *Robotics and Autonomous Systems*, vol. 62, no. 12, pp. 1777 – 1789, 2014.

[22] P. Manoonpong, U. Parlitz, and F. Wörgötter, "Neural control and adaptive neural forward models for insect-like, energy-efficient, and adaptable locomotion of walking machines," *Frontiers in Neural Circuits*, vol. 7, no. 12, 2013.

[23] J. Lee, S. Sponberg, O. Loh, A. Lamperski, R. Full, and N. Cowan, "Templates and anchors for antenna-based wall following in cockroaches and robots," *Robotics, IEEE Transactions on*, vol. 24, no. 1, pp. 130–143, Feb 2008.

[24] P. Holmes, R. Full, D. Koditschek, and J. Guckenheimer, "The dynamics of legged locomotion: Models, analyses, and challenges," *SIAM Review*, vol. 48, no. 2, pp. 207–304, 2006.

[25] J. Yu, M. Tan, J. Chen, and J. Zhang, "A survey on cpg-inspired control models and system implementation," *Neural Networks and Learning Systems, IEEE Transactions on*, vol. 25, no. 3, pp. 441–456, March 2014.

[26] A. V. Hill, "The heat of shortening and the dynamic constants of muscle," *Proceedings of the Royal Society of London. Series B - Biological Sciences*, vol. 126, no. 843, pp. 136–195, 1938.

[27] F. Zajac, "Muscle and tendon: properties, models, scaling, and application to biomechanics and motor control." *Crit Rev Biomed Eng*, vol. 17, no. 4, pp. 359–411, 1989.

[28] M. A. Smith, A. Ghazizadeh, and R. Shadmehr, "Interacting adaptive processes with different timescales underlie short-term motor learning," *PLoS Biol*, vol. 4, no. 6, p. e179, 05 2006.

[29] D. M. Wolpert, J. Diedrichsen, and J. R. Flanagan, "Principles of sensorimotor learning," *Nat Rev Neurosci*, vol. 12, no. 12, pp. 739–751, Dec. 2011.

[30] P. Gregorio, M. Ahmadi, and M. Buehler, "Design, control, and energetics of an electrically actuated legged robot," *Systems, Man, and Cybernetics, Part B: Cybernetics, IEEE Transactions on*, vol. 27, no. 4, pp. 626 –634, aug 1997.

[31] K. C. Galloway, "Passive variable compliance for dynamic legged robots," PhD thesis, University of Pennsylvania, 2010.

[32] A. J. Ijspeert, "Central pattern generators for locomotion control in animals and robots: A review," *Neural Networks*, vol. 21, no. 4, pp. 642 – 653, 2008, robotics and Neuroscience.

[33] C. Semini, V. Barasuol, T. Boaventura, M. Frigerio, and J. Buchli, "Is active impedance the key to a breakthrough for legged robots?" in *International Symposium of Robotics Research (ISRR)*, 2013.

[34] R. Ham, T. Sugar, B. Vanderborght, K. Hollander, and D. Lefeber, "Compliant actuator designs," *Robotics Automation Magazine, IEEE*, vol. 16, no. 3, pp. 81 –94, september 2009.

[35] D. Kingsley, R. Quinn, and R. E. Ritzmann, "A cockroach inspired robot with artificial muscles," in *Intelligent Robots and Systems, 2006 IEEE/RSJ International Conference on*, 2006, pp. 1837–1842.

[36] E. Garcia and P. de Santos, "On the improvement of walking performance in natural environments by a compliant adaptive gait," *Robotics, IEEE Transactions on*, vol. 22, no. 6, pp. 1240–1253, 2006.

[37] Y. Fukuoka, H. Kimura, and A. H. Cohen, "Adaptive dynamic walking of a quadruped robot on irregular terrain based on biological concepts," *The International Journal of Robotics Research*, vol. 22, no. 3-4, pp. 187–202, 2003.

[38] B. Webb, "Neural mechanisms for prediction: do insects have forward models?" *Trends in Neurosciences*, vol. 27, no. 5, pp. 278 – 282, 2004.

[39] P. Cormie, M. McGuigan, and R. Newton, "Developing maximal neuromuscular power," *Sports Medicine*, vol. 41, no. 1, pp. 17–38, 2011.

[40] A. A. Biewener, *Biomechanics– structures and systems: a practical approach*. Oxford University Press, 1992.

[41] J. H. LONG, "Muscles, elastic energy, and the dynamics of body stiffness in swimming eels," *American Zoologist*, vol. 38, no. 4, pp. 771–792, 1998.

[42] R. P. Kukillaya and P. Holmes, "A model for insect locomotion in the horizontal plane: Feedforward activation of fast muscles, stability, and robustness," *Journal of Theoretical Biology*, vol. 261, no. 2, pp. 210 – 226, 2009.

[43] D. M. Dudek and R. J. Full, "Passive mechanical properties of legs from running insects," *The Journal of Experimental Biology*, vol. 209, no. 8, pp. 1502–1515, 2006.

[44] D. V. Lee, M. P. McGuigan, E. H. Yoo, and A. A. Biewener, "Compliance, actuation, and work characteristics of the goat foreleg and hindleg during level, uphill, and downhill running," *Journal of Applied Physiology*, vol. 104, no. 1, pp. 130–141, January 2008.

[45] A. M. Carroll, D. V. Lee, and A. A. Biewener, "Differential muscle function between muscle synergists: long and lateral heads of the triceps in jumping and landing goats (capra hircus)," *Journal of Applied Physiology*, vol. 105, no. 4, pp. 1262–1273, 2008.

[46] M. A. Daley, G. Felix, and A. A. Biewener, "Running stability is enhanced by a proximo-distal gradient in joint neuromechanical control," *Journal of Experimental Biology*, vol. 210, no. 3, pp. 383–394, 2007.

[47] A. A. BIEWENER, "Muscle function in vivo: A comparison of muscles used for elastic energy savings versus muscles used to generate mechanical power1," *American Zoologist*, vol. 38, no. 4, pp. 703–717, 1998.

[48] M. A. Daley and A. A. Biewener, "Muscle force-length dynamics during level versus incline locomotion: a comparison of in vivo performance of two guinea fowl ankle extensors," *Journal of Experimental Biology*, vol. 206, no. 17, pp. 2941–2958, 2003.

[49] T. J. Roberts, R. L. Marsh, P. G. Weyand, and C. R. Taylor, "Muscular force in running turkeys: The economy of minimizing work," *Science*, vol. 275, no. 5303, pp. 1113–1115, 1997.

[50] G. B. Gillis, J. P. Flynn, P. McGuigan, and A. A. Biewener, "Patterns of strain and activation in the thigh muscles of goats across gaits during level locomotion," *Journal of Experimental Biology*, vol. 208, no. 24, pp. 4599–4611, 2005.

[51] M. P. McGuigan, E. Yoo, D. V. Lee, and A. A. Biewener, "Dynamics of goat distal hind limb muscletendon function in response to locomotor grade," *Journal of Experimental Biology*, vol. 212, no. 13, pp. 2092–2104, 2009.

[52] D. V. Lee and A. A. Biewener, "Bigdog-inspired studies in the locomotion of goats and dogs," *Integrative and Comparative Biology*, vol. 51, no. 1, pp. 190–202, 2011.

[53] M. A. Daley and A. A. Biewener, "Leg muscles that mediate stability: mechanics and control of two distal extensor muscles during obstacle negotiation in the guinea fowl," *Philosophical Transactions of the Royal Society B: Biological Sciences*, vol. 366, no. 1570, pp. 1580–1591, 2011.

[54] M. A. Daley and A. Biewener, "Running over rough terrain reveals limb control for intrinsic stability," *Proceedings of the National Academy of Sciences*, vol. 103, no. 42, pp. 15 681–15 686, 2006.

[55] T. J. Roberts, "The integrated function of muscles and tendons during locomotion," *Comparative Biochemistry and Physiology Part A: Molecular & Integrative Physiology*, vol. 133, no. 4, pp. 1087 – 1099, 2002.

[56] D. A. McCrea and I. A. Rybak, "Organization of mammalian locomotor rhythm and pattern generation," *Brain Research Reviews*, vol. 57, no. 1, pp. 134 – 146, 2008.

[57] P. Arena, L. Fortuna, M. Frasca, and G. Sicurella, "An adaptive, self-organizing dynamical system for hierarchical control of bio-inspired locomotion," *Systems, Man, and Cybernetics, Part B: Cybernetics, IEEE Transactions on*, vol. 34, no. 4, pp. 1823–1837, Aug 2004.

[58] P. Manoonpong, F. Pasemann, and F. Wörgötter, "Sensor-driven neural control for omnidirectional locomotion and versatile reactive behaviors of walking machines," *Robotics and Autonomous Systems*, vol. 56, no. 3, pp. 265 – 288, 2008.

[59] S. Heitmann, M. Breakspear, and N. Ferns, "Muscle co-contraction modulates damping and joint stability in a three-link bio mechanical limb," *Frontiers in Neurorobotics*, vol. 5, no. 5, 2012.

[60] X. Xiong, F. Wörgötter, and P. Manoonpong, "A neuromechanical controller of a hexapod robot for walking on sponge, gravel and snow surfaces," in *Advances in Artificial Life. Proceedings of the 11th European Conference on Artificial Life ECAL 2013*, 2013, pp. 989–996.

[61] N. Hogan and S. P. Buerger, *Impedance and Interaction Control*, ser. Robotics and Automation Handbook, T.R.Kurfess, Ed. CRC Press, 2004, vol. Chapter 19.

[62] M. H. Dickinson, C. T. Farley, R. J. Full, M. A. R. Koehl, R. Kram, and S. Lehman, "How animals move: An integrative view," *Science*, vol. 288, no. 5463, pp. 100–106, 2000.

[63] X. Xiong, F. Wörgötter, and P. Manoonpong, "Virtual agonist-antagonist mechanisms produce biological muscle-like functions: An application for robot joint control," *Industrial Robot: An International Journal*, vol. 41, no. 4, pp. 340 – 346, 2014.

[64] S. Zill, J. Schmitz, and A. Bschges, "Load sensing and control of posture and locomotion," *Arthropod Structure & Development*, vol. 33, no. 3, pp. 273 – 286, 2004, arthropod Locomotion Systems: from Biological Materials and Systems to Robotics.

[65] J. Pratt, C.-M. Chew, A. Torres, P. Dilworth, and G. Pratt, "Virtual model control: An intuitive approach for bipedal locomotion," *The International Journal of Robotics Research*, vol. 20, no. 2, pp. 129–143, 2001.

[66] M. Hutter, C. Remy, M. Hoepflinger, and R. Siegwart, "Scarleth: Design and control of a planar running robot," in *Intelligent Robots and Systems (IROS), 2011 IEEE/RSJ International Conference on*, Sept 2011, pp. 562–567.

[67] R. Der and G. Martius, "The lpzrobots simulator," in *The Playful Machine*, ser. Cognitive Systems Monographs. Springer Berlin Heidelberg, 2012, vol. 15, pp. 293–308.

[68] M. Raibert, K. Blankespoor, G. Nelson, R. Playter, and the BigDog Team, "Bigdog, the rough-terrain quadruped robot," in *Proceedings of the 17th IFAC World Congress, 2008*, M. J. Chung, Ed., vol. 17, no. 1, 2008, pp. 10 822–10 825.

[69] A. K. Lappin, J. A. Monroy, J. Q. Pilarski, E. D. Zepnewski, D. J. Pierotti, and K. C. Nishikawa, "Storage and recovery of elastic potential energy powers ballistic prey capture in toads," *Journal of Experimental Biology*, vol. 209, no. 13, pp. 2535–2553, 2006.

[70] R. M. Alexander, *Principles of Animal Locomotion*. Princeton University Press, 2003.

[71] G. A. Pratt, "Low impedance walking robots," *Integrative and Comparative Biology*, vol. 42, no. 1, pp. 174–181, 2002.

[72] P. Arena, L. Fortuna, M. Frasca, L. Patane, and M. Pavone, "Realization of a cnn-driven cockroach-inspired robot," in *Circuits and Systems, 2006. ISCAS 2006. Proceedings. 2006 IEEE International Symposium on*, May, pp. 2649–2652.

[73] A. Rönnau, G. Heppner, M. Nowicki, and R. Dillmann, "Lauron v: A versatile six-legged walking robot with advanced maneuverability," in *Advanced Intelligent Mechatronics (AIM), 2014 IEEE/ASME International Conference on*, July 2014, pp. 82–87.

[74] B. Vanderborght, A. Albu-Schaeffer, A. Bicchi, E. Burdet, D. Caldwell, R. Carloni, M. Catalano, O. Eiberger, W. Friedl, G. Ganesh, M. Garabini, M. Grebenstein, G. Grioli, S. Haddadin, H. Hoppner, A. Jafari, M. Laffranchi, D. Lefeber, F. Petit, S. Stramigioli, N. Tsagarakis, M. V. Damme, R. V. Ham, L. Visser, and S. Wolf, "Variable impedance actuators: A review," *Robotics and Autonomous Systems*, vol. 61, no. 12, pp. 1601 – 1614, 2013.

[75] J. Proctor and P. Holmes, "Reflexes and preflexes: on the role of sensory feedback on rhythmic patterns in insect locomotion," *Biological Cybernetics*, vol. 102, no. 6, pp. 513–531, 2010.